

Article

Contribution of Different Pretreatments to the Thermal Stability and UV Resistance Performance of Cellulose Nanofiber Films

Lianxin Luo ^{1,2}, Xuchong Wang ^{1,2}, Sheng Zhang ^{1,2}, Xiaojun Yuan ^{1,2}, Mingfu Li ^{3,4,*}  and Shuangfei Wang ^{1,2,*} 

- ¹ College of Light Industry and Food Engineering, Guangxi University, Nanning 530004, China; luolianxin@gxu.edu.cn (L.L.); 1916301029@st.gxu.edu.cn (X.W.); 1916301042@st.gxu.edu.cn (S.Z.); 1816301034@st.gxu.edu.cn (X.Y.)
- ² Guangxi Key Laboratory of Clean Pulp & Papermaking and Pollution Control, Guangxi University, Nanning 530004, China
- ³ University of Chinese Academy of Sciences, Beijing 100049, China
- ⁴ Ningbo Institute of Materials Technology & Engineering, Chinese Academy of Sciences, Ningbo 315201, China
- * Correspondence: limingfu@nimte.ac.cn (M.L.); wangsf@gxu.edu.cn (S.W.)

Abstract: Hot water (HW), green liquor (GL), and sodium chlorite (SC) pretreatments were used to pretreat sugarcane bagasse (SCB) and spruce (SP) and then to prepare cellulose nanofibers (CNFs) through high-pressure homogenization to explore the effect of physicochemical properties on the thermal stability and ultraviolet (UV) resistance performance of CNF films. The results indicated that the lignin content of HW-pretreated CNFs was higher than that of GL- and SC-pretreated CNFs, and the hemicellulose content of HW-pretreated CNFs was lower than that of GL- and SC-pretreated CNFs. The synergy of lignin and hemicellulose impacted the thermal stability of CNF films. The thermal stability of all the SP CNF films was higher than that of all the SCB CNF films. Hot water pretreatment improved the thermal stability of CNF films, and green liquor and sodium chlorite pretreatment decreased the thermal stability of CNF films. The highest thermal stability of SP-HW CNF films reached 392 °C, which was 5.4% higher than that of SP-SC CNF films. Furthermore, the ultraviolet resistance properties of different CNF films were as follows: SCB-HW > SCB-GL > SCB-SC and SP-HW > SP-GL > SP-SC. Green liquor pretreatment is an effective method to prepare CNFs. Conclusively, this research provides a basic theory for the preparation of CNFs and allows the improvement of CNF films in the application of thermal stability management and UV resistance fields.

Keywords: cellulose nanofiber; pretreatment; lignin; hemicellulose; physicochemical properties



Citation: Luo, L.; Wang, X.; Zhang, S.; Yuan, X.; Li, M.; Wang, S. Contribution of Different Pretreatments to the Thermal Stability and UV Resistance Performance of Cellulose Nanofiber Films. *Coatings* **2021**, *11*, 247. <https://doi.org/10.3390/coatings11020247>

Academic Editor:
Alessandro Pezzella

Received: 5 January 2021
Accepted: 11 February 2021
Published: 19 February 2021

Publisher's Note: MDPI stays neutral with regard to jurisdictional claims in published maps and institutional affiliations.



Copyright: © 2021 by the authors. Licensee MDPI, Basel, Switzerland. This article is an open access article distributed under the terms and conditions of the Creative Commons Attribution (CC BY) license (<https://creativecommons.org/licenses/by/4.0/>).

1. Introduction

In recent years, the overexploitation and utilization of global fossil energy and fuels has led to environmental changes and energy shortages. Therefore, there is increasing interest for sustainable and environmentally friendly materials research [1,2]. Cellulose nanofibers (CNFs) have become a promising renewable material because of their unique structure, excellent performance, and natural abundance. It is widely found in plants and considered a nontoxic, degradable, and low-cost material, so it is a good substitute for synthesizing many products [3,4]. CNFs can be used to prepare pollution-free product components, such as membrane electrode assemblies, organic light-emitting diodes, writable touch screens, energy storage materials, and eco-friendly fabric softeners [5–8]. Thermal instability is the main problem of biomass materials because their components have a low melting temperature. Therefore, these electronic components are easily destroyed when they encounter high temperatures and need to be annealed or sterilized [9]. CNFs can be

combined with other wood material components to produce a hybrid superlattice structure, reduce their thermal conductivity, and become a thermoelectric energy-harvesting material.

The thermal stability of CNFs is closely related to the lignin and hemicellulose in plant fibers [10]. Lignin and hemicellulose act as binders and fillers in lignocellulosic raw materials, and many cellulose molecular chains combine to form fiber bundles [11]. Lignin is one of the main components in lignocellulosic raw materials [12]. It is a natural high molecular weight polymer with a three-dimensional structure that is formed by connecting a phenylpropane structure through ether and carbon-carbon bonds [13]. Lignin can increase the water contact angle of cellulose fiber films, reduce their water absorption capacity, and improve the thermal stability and UV barrier properties of cellulose fiber-based films [14,15]. The degradation of wood fiber is a complex process involving a series of continuous reactions, and its thermal stability depends on the chemical composition, fiber size, crystal structure, and number of intermolecular and intramolecular hydrogen bonds. Nair et al. investigated the effect of lignin on the thermal stability of CNFs, indicating that the presence of lignin significantly improved the thermal stability of CNFs [16].

The preparation methods for CNFs also impact on their thermal stability. Pretreatments can change the cell wall structure and composition of lignocellulose, reduce energy consumption during the preparation of CNFs, and increase the yield of CNFs [17–19]. At present, the main pretreatments include acid, alkali, hot water, organosolv, and ionic liquid pretreatments [1,20,21]. Compared to gamma-valerolactone/water [22], catalyzed chemical oxidation [23] and organosolv pretreatment [24] were used to pretreat lignocellulose and prepare CNFs, and hot water pretreatment as a green and environmental method can save chemical reagent consumption [25]. Furthermore, green liquor as a kind of alkaline liquor mainly consists of sodium carbonate and sodium sulfide, which is the liquor recovered after the combustion of black liquor in the recovery boiler of the Kraft pulp mill. Green liquor was used to pretreat lignocellulosic biomass can decrease the overall cost for the pretreatment process [26], which could also alleviate the discharge of pulping wastewater. Therefore, using the green liquor pretreated lignocellulose to prepare CNFs can realize the reusability of the wastewater in pulp and papermaking. However, there is a lack of using green liquor pretreatment to pretreat lignocellulose and then prepare CNFs, and to further investigate the effect of pretreatment on the physicochemical properties of CNFs.

Therefore, in this work, hot water, green liquor and sodium chlorite were used to pretreat sugarcane bagasse and spruce and then prepare CNFs by high-pressure homogenization. Component analysis, transmission electron microscope (TEM), Fourier transform infrared spectroscopy (FTIR), thermogravimetric (TG), and ultraviolet (UV) spectroscopy were used to analyze the effect of different pretreatments on the physicochemical properties of the CNFs and CNF films. Furthermore, the effect of residual lignin and hemicellulose content on the thermal stability and UV resistance of CNF films was also investigated. This research provides the basic theory for CNFs in the application of thermal management and UV resistance fields.

2. Experiments

2.1. Materials

Sugarcane bagasse was provided by Guangxi Guitang (Group) Co., Ltd. (Guigang, China), spruce originated from European spruce (Alps, Bavaria, Germany). Sodium sulfide, sodium carbonate, sodium hydroxide, sodium chlorite (SC), glacial acetic acid, and sulfuric acid were purchased from Tianjin Zhiyuan Chemical Reagent Co., Ltd. (Tianjin, China).

2.2. Pretreatments

The scheme of lignocellulose pretreatments was shown in Figure 1. A six-pot digester (2201-6, Anderson Greenwood Instruments, South Plainfield, NJ, USA) was used for pretreatment experiments. For the hot water pretreatment process, 30 g of sugarcane bagasse (spruce) raw material was placed into a 1 L tank, 450 mL of water was added, and the pretreatment temperature and residence time were 170 °C and 90 min, respectively.

For the simulated green liquor pretreatment process, 30 g of sugarcane bagasse (spruce) raw material was placed into a 1 L tank, 180 mL of green liquor was added, and the pretreatment temperature and residence time were 120 °C and 60 min, respectively. The sulfidity and total alkali were 25% and 16% (based on Na₂O), respectively. The pretreated solids were washed with hot water for further use. Furthermore, the raw materials were pretreated with sodium chlorite [27,28]. Two grams of sugarcane bagasse (spruce) raw material was placed into a 250 mL conical flask, 200 mL distilled water was added into the conical flask, and a constant temperature was maintained in a water bath at 75 °C. One milliliter of glacial acetic acid and 1.2 g of sodium chlorite were added to the liquor every 1 h, and the reaction time was 3 h. After the reaction was completed, the solid was washed with hot water for further use.

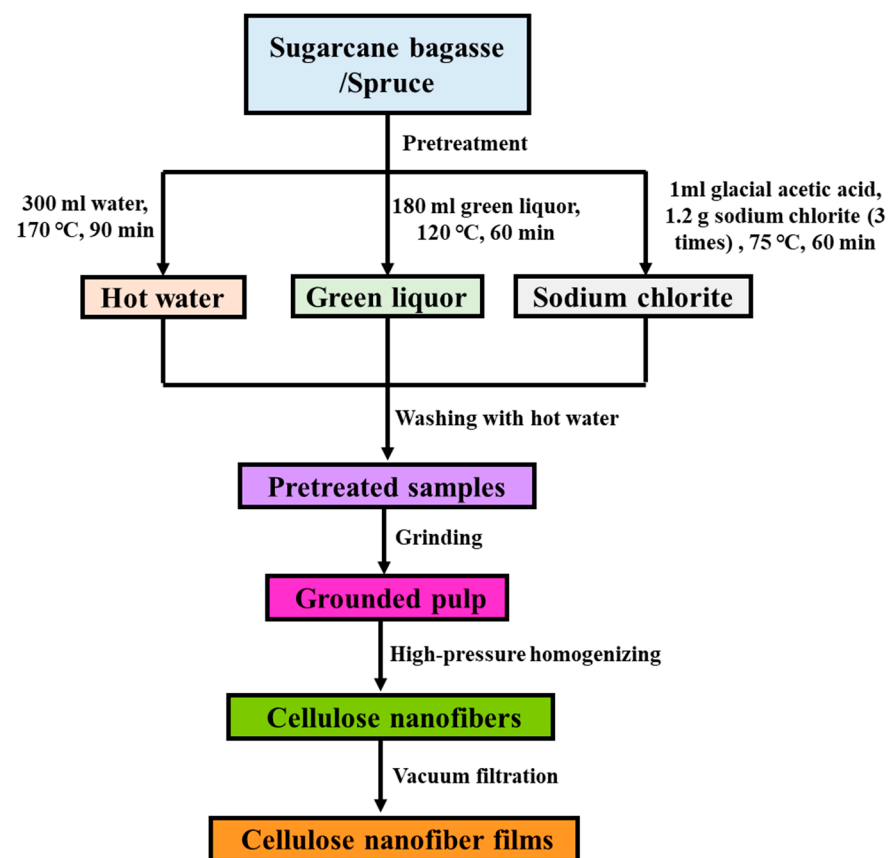


Figure 1. The scheme of lignocellulose pretreatments and cellulose nanofibers (CNFs) films' preparation.

2.3. Preparation of Cellulose Nanofibers

The pretreated sugarcane bagasse and spruce fibers were used to disc mills, and the grinding distances were 0.2, 0.1, and 0.1 μm, respectively, to prepare grounded pulp. Then, the ground pulp was pretreated by a high-pressure homogenizer (M-110EH-30, Microfluidizer, Westwood, CA, USA). The pulp concentration was 1%. First, the pulp was homogenized 20 times at a pressure of 350 bar and a hole diameter of 200 μm in the high-pressure homogenizer. Then, the pulp was homogenized 10 times at a pressure of 1500 bar and a pore size of 87 μm to obtain the CNFs. The CNF films were prepared by the vacuum filtration method [5]. The prepared CNFs were stirred with a magnetic stirrer to make them fully dispersed. The dispersed CNFs were converted into CNF films with a diameter of 90 mm and mass of 0.4 g and put into an automatic molding dryer (BBS-2, ESTANITHAAGE, Berlin, Germany) at 75 °C for 15 min. The prepared CNFs were nominated as hot water pretreated sugarcane bagasse CNFs (SCB-HW), green liquor pretreated sugarcane bagasse CNFs (SCB-GL), and sodium chlorite pretreated sugarcane bagasse CNFs (SCB-SC). The prepared spruce CNFs were named hot water pretreated

spruce CNFs (SP-HW), green liquor pretreated spruce CNFs (SP-GL), and sodium chlorite pretreated spruce CNFs (SP-SC).

2.4. Chemical Composition Analysis of Cellulose Nanofibers

CNFs (0.25 g) were added into an autoclave, 1.5 mL of 72% concentrated sulfuric acid was added, and then carbonized at 30 °C for 1 h. After carbonization, 43 mL of distilled water was added, and an autoclave was used to react at 121 °C for 1 h. After the reaction was completed, the solids and filtrate were separated by filtration, and the solids were washed with distilled water to neutral. Then, the solid was dried at 105 °C for 4 h to obtain acid-insoluble lignin (Klason lignin). The acid-soluble lignin and carbohydrate (glucose and xylose) in the liquor were determined by a UV VIS spectrophotometer (Analytik Jena, Jena, Germany) and high-performance liquid chromatography (Agilent, 1260, Palo Alto, CA, USA), respectively, according to the previous report [29,30]. Each experiment was performed twice, and the statistical analysis was conducted with MS Excel 2016. The average values and confidence interval (level of significance = 0.05) were determined.

2.5. Characterization of Cellulose Nanofibers

Transmission electron microscope (TEM) analysis: The samples were prepared for TEM analysis. The CNFs were dispersed in water with a mass concentration of 0.05%, then a piece of filter paper was placed in a petri dish, a copper mesh was placed on the filter paper, and a certain amount of CNFs dispersion was dropped on the TEM copper grid and dried at room temperature for 12 h. Then, 1 mL of staining agent (2% phosphotungstic acid) was dropped on the copper mesh, the droplets completely covered the copper mesh, and it was put in a dark box for 30 min. Finally, the copper mesh was placed at room temperature to obtain CNFs dyed samples. A JEM-1200EX transmission electron microscope (JEOL, Tokyo, Japan) was used to analyze the CNF morphology. The test voltage and the current were 120 kV and 100 μ A, respectively, and the magnification was 80,000 times for test analysis.

Fourier transform infrared (FTIR) spectroscopy: A German Bruker Tensor II was used for FT-IR measurement (Bruker, Karlsruhe, Germany) of CNFs. One milligram of sample and 100 mg of potassium bromide were mixed to prepare circular slices by pressing and then put into an infrared analyzer for testing. The scanning range was 4000–400 cm^{-1} , the number of scanning cycles was 32, and the scanning frequency was 4 cm^{-1} [31].

XPS analysis: The prepared CNF membrane was cut into a size of 0.5 \times 0.5 cm^2 , fixed on a sample device, and placed into an X-ray photoelectron spectrometer to analyze the sample. An X-ray spectrometer (Axis Ultra DLD, KRATOS, Manchester, UK) was used to analyze the surface element content of the CNFs. The working vacuum of the analysis was 5 \times 10⁻⁹ torr, the monochromatic Al K α source energy was 1486.6 eV (5 mA \times 15 kV), and the beam spot size was 700 \times 300 μm^2 . A CAE scanning mode was adopted. Full-spectrum scan: The pass energy was 160 eV; the narrow-spectrum scan pass energy was 40 eV, and the number of scans was 3. The surface lignin content (SLC) of CNFs was calculated according to formula (1) [32].

$$\text{SLC (\%)} = \frac{O/C_{\text{sample}} - O/C_{\text{carbohydrate}}}{O/C_{\text{lignin}} - O/C_{\text{carbohydrate}}} \quad (1)$$

The values of $O/C_{\text{carbohydrate}}$ and O/C_{lignin} were 0.83 and 0.33, respectively.

X-ray diffraction (XRD) analysis: The prepared CNF film was cut into a size of 2 \times 2 cm^2 , placed into the groove of the glass sample plate, and analyzed with a high-resolution X-ray diffractometer (SMARTLAB 3KW, Tokyo, Japan). The scanning range was 5°–50° at a speed of 0.25 steps, each step was 10 s, the scanning speed was 0.18 min, and the step length was 0.018° for analysis. The crystallinity (CrI) of CNFs was calculated according to the Segal method [33] as follows.

$$\text{CrI (\%)} = \frac{(I_{002} - I_{am})}{I_{002}} \times 100\% \quad (2)$$

where I_{002} is the intensity of the diffraction peak at $2\theta = 22^\circ$ and I_{am} is the intensity of the diffraction peak at $2\theta = 18^\circ$.

2.6. Thermogravimetry (TGA) Analysis

The CNF samples were vacuum dried at 40°C for 24 h, and then thermogravimetric analysis of the CNFs was performed with a synchronous thermal analyzer (STA 449F5, NETZSCH, Selbu, Germany) [27]. The mass of the sample was 10 mg, the nitrogen flow and heating rate were $40\text{ mL}\cdot\text{min}^{-1}$ and $10\text{ K}\cdot\text{min}^{-1}$, respectively, and the heating temperature ranged from 25 to 700°C .

2.7. UV Absorption Performance

The size of the prepared CNF films was $30 \times 12\text{ mm}^2$, and they were spectrally scanned using an ultraviolet-visible spectrophotometer (ANALYTIK Jena, Jena, Germany) with a scanning wavelength of 190–900 nm [34,35].

3. Results and Discussion

3.1. Chemical Composition of CNFs

The chemical composition analysis of different CNFs is shown in Table 1. The lignin content in hot water-pretreated SCB and spruce CNFs was higher than that in green liquor- and sodium chlorite-pretreated SCB and spruce CNFs. For example, the lignin contents of SCB-HW, SCB-GL, and SCB-SC were 22.5%, 8.4%, and 1.8%, respectively. These results indicate that the removal of lignin in sugarcane bagasse and spruce pretreated with green liquor was higher than that by hot water pretreatment. Furthermore, the lignin content in SCB-HW (SCB-GL) was lower than that in SP-HW (SP-GL) due to the compact structure of the high lignin content in the spruce cell wall, which resulted in the lignin difficultly removed under mild pretreatment conditions. After hot water pretreatment, the hemicellulose content in the SCB-HW and SP-HW seriously decreased, the lignin content in SCB-HW and SP-HW slightly decreased, indicating that hot water pretreatment mainly removed the hemicellulose from the CNFs.

Table 1. Chemical composition of different CNFs. SCB—sugarcane bagasse; SCB-HW—hot water pretreated sugarcane bagasse CNFs; SCB-GL—green liquor pretreated sugarcane bagasse CNFs; SCB-SC—sodium chlorite pretreated sugarcane bagasse CNFs; SP—spruce; SP-HW—hot water pretreated spruce CNFs; SP-GL—green liquor pretreated spruce; SP-SC—sodium chlorite pretreated spruce CNFs.

Samples	Cellulose (%)	Hemicellulose (%)	Lignin (%)
SCB	41.7 ± 0.6	26.6 ± 0.4	24.4 ± 0.7
SCB-HW	45.4 ± 0.6	5.5 ± 0.6	22.5 ± 0.6
SCB-GL	46.9 ± 0.5	7.6 ± 0.4	8.4 ± 0.3
SCB-SC	62.6 ± 0.3	3.5 ± 0.6	1.8 ± 0.3
SP	43.6 ± 0.2	23.9 ± 0.6	28.6 ± 0.7
SP-HW	47.4 ± 0.2	7.5 ± 0.6	26.0 ± 0.4
SP-GL	49.2 ± 0.2	9.1 ± 0.5	15.1 ± 0.7
SP-SC	55.6 ± 0.4	4.0 ± 0.5	2.8 ± 0.6

3.2. Photography and TEM Analysis

The photograph of different pretreated CNF films is shown in Figure 2, indicating the colors of different CNF films changed from brown to white. The hot water-pretreated SCB and SP CNF films were darker than the green liquor- and sodium chlorite-pretreated CNF films, due to the lignin content in the hot water-pretreated CNFs was higher than that in the green liquor- and sodium chlorite-pretreated CNFs. Compared to the SCB-HW (or SCB-GL) CNF films, the color of SP-HW (or SP-GL) CNF films was brighter, possibly due to the more unsaturated bonds of lignin was formed in SCB-HW (or SCB-GL) CNFs during hot water (or green liquor) pretreatment led to the color of SCB-HW (or SCB-GL) CNF films

was darker. The SCB-SC CNF films was brighter than SP-SC CNF films due to the lignin of SCB-SC CNF was almost completely removed during sodium chlorite pretreatment.

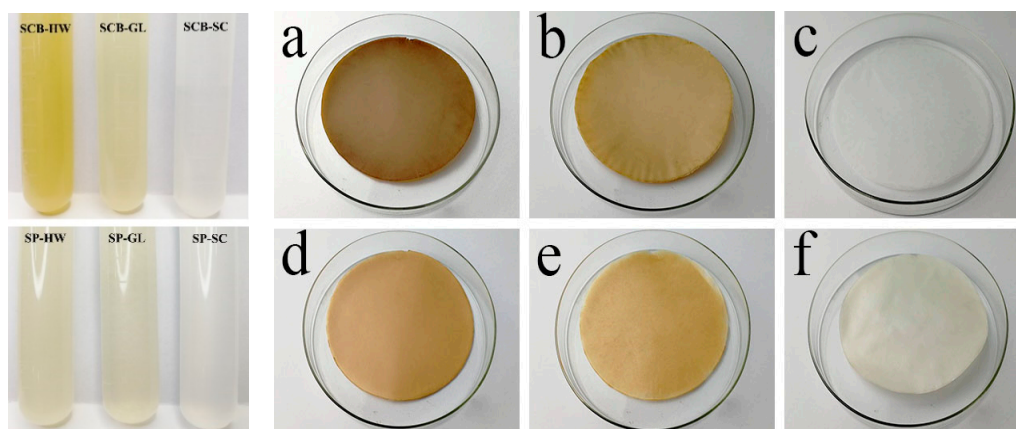


Figure 2. Photographs of different CNF films ((a) SCB-HW, (b) SCB-GL, (c) SCB-SC, (d) SP-HW, (e) SP-GL, (f) SP-SC).

TEM analysis of different pretreated CNFs is shown in Figure 3, indicating the size and morphology of CNFs were different. The diameters of SCB-HW, SCB-GL, and SCB-SC were 15.3, 13.7, and 12.8 nm, respectively. The diameters of SP-HW, SP-GL, and SP-SC were 19.5, 17.2, and 14.7 nm, respectively. Compared to hot water pretreatment, the green liquor- and sodium chlorite-pretreated CNFs were easily dispersed in water because more lignin was removed by the green liquor and sodium chlorite pretreatment, leading to more hydrophilic groups of CNFs, such as hydroxyl and carboxyl groups, exposed on the surface [36]. Furthermore, the diameter of sugarcane bagasse and spruce CNFs was different possibly due to the size of the original sugarcane bagasse raw material fiber was smaller than that of spruce raw material fiber.

3.3. FTIR Analysis

FTIR spectroscopy is widely used to investigate the change of functional groups in lignocellulose under different processing conditions [37]. The FTIR spectra of different CNFs are shown in Figure 4a, b. The peak intensity in FTIR was calibrated using the peak at 1110 cm^{-1} as a reference peak [38]. It can be seen that the peak at 3356 cm^{-1} was assigned to the intermolecular O–H stretching vibration on the cellulose carbon skeleton [38], the peak at 2860 cm^{-1} was assigned to the C–H absorption peaks of methyl, methylene, and methine [39], and the peak at 1730 cm^{-1} was assigned to the absorption peak of non-conjugated carbonyl with an aromatic ring and its ester and lactone. Compared to the SCB-HW and SP-HW, the peak intensities of the O–H stretching vibration and nonconjugated carbonyl in SCB-GL and SP-GL were decreased, possibly due to the oxidation and degradation of a large amount of lignin during the pretreatment process. The peak intensity of the O–H stretching vibration in SCB-SC and SP-SC was increased because the hydroxyl group was oxidized to a carboxyl group during the pretreatment process. The peak at 1700 cm^{-1} was assigned to the ester bond of C=O, which is usually derived from the acetyl group in hemicellulose and the linkage between lignin and hemicellulose [40]. The peak at 1644 cm^{-1} was assigned to the conjugated carbonyl of lignin [41], and the characteristic peaks at 1604 cm^{-1} , 1506 cm^{-1} , 1462 cm^{-1} , and 1422 cm^{-1} were assigned to the aromatic ring of lignin [19,42]. Compared to the SCB-HW and SP-HW, these intensities of peaks in SCB-SC, SCB-GL, SP-SC, and SP-GL decreased or disappeared due to the removal of lignin after different pretreatments. The intensity of the peak at 809 cm^{-1} decreased due to stretching of the homocyclic ring of mannose residues, which was related to hemicellulose removal.

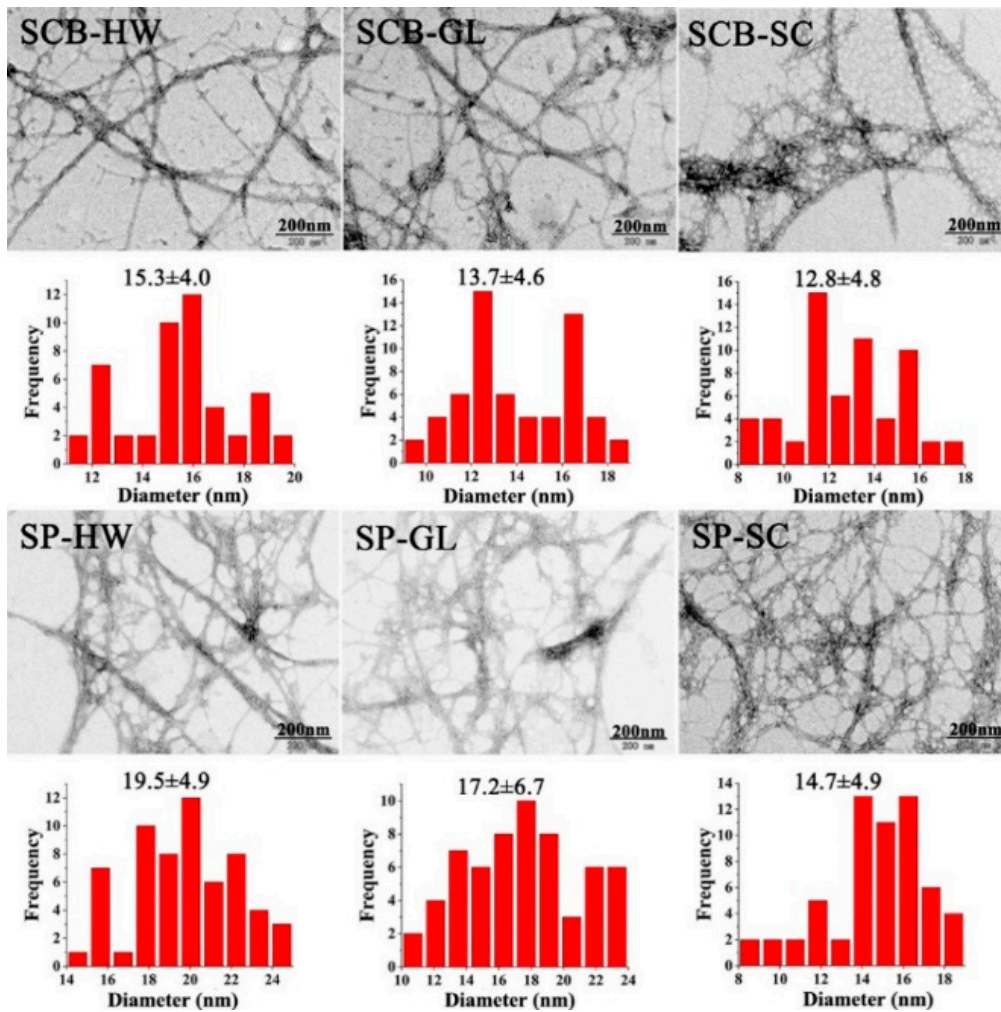


Figure 3. TEM and size analysis of CNFs.

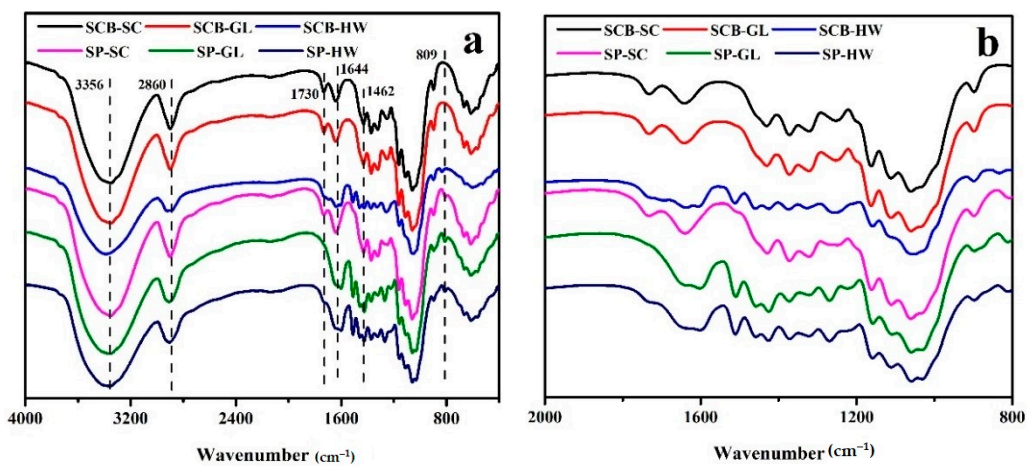


Figure 4. FTIR spectroscopy of CNFs (a) 4000–400 cm^{-1} (b) 2000–800 cm^{-1} .

3.4. XPS Analysis

To study the effect of pretreatment on the surface chemical properties of CNF films, XPS was used to analyze the C, O, and S elements on the surface of different CNF films [43,44], as shown in Table 2. Compared to hot water-pretreated CNF films, the

content of C decreased, while the content of O increased in green liquor-pretreated CNF films. The small increase of sulfur due to S^{2-} or HS^- was attached on the surface of fiber during the green liquor pretreatment process. The increase in the oxygen-carbon ratio may be due to the lignin being removed during the green liquor pretreatment process. The content of C decreased, and the content of O increased in SCB-SC and SP-SC, leading to an increase in the ratio of O/C. The increase in the oxygen-carbon ratio due to the amount of lignin was removed by sodium chlorite pretreatment, resulting in more carbohydrates being exposed on the surface of the fiber. The change in the oxygen-carbon ratio impacted the surface lignin content (SLC) of the CNF films. Compared to hot water pretreated CNFs films, the SLC of green liquor and sodium chlorite pretreated CNFs films decreased, the SLC in green liquor pretreated CNFs films was higher than sodium chlorite pretreated CNFs films, due to a large amount of lignin being removed by sodium chlorite pretreatment. Furthermore, the SLC of SP-HW CNF films was higher than that of SCB-HW CNF films because the lignin content in SP-HW CNFs was higher than that in SCB-HW CNF films (Table 1).

Table 2. Surface element analysis of CNFs films.

Samples	C (%)	O (%)	S (%)	O/C	SLC (%)
SCB-HW	69.4	30.4	0.17	0.44	78
SCB-GL	66.5	33.2	0.23	0.50	66
SCB-SC	64.8	35.0	0.19	0.54	58
SP-HW	71.6	28.1	0.15	0.39	87
SP-GL	68.2	31.6	0.26	0.46	74
SP-SC	59.1	40.6	0.20	0.69	28

The change in lignin content on the surface of CNFs can also be characterized by the change in C1s. C1s can be divided into three combined types of C1 (C–C), C2 (C–O), C3 (O–C–O or C=O) [44–46], as shown in Figure 5. The binding energy of C1 at 285 eV was derived from lignin and extracts, the binding energy of C2 at 286.5 eV was derived from carbohydrates, and the binding energy of C3 at 288–288.5 eV was derived from lignin and fiber oxidation products [44]. The percentages of C1, C2, and C3 are shown in Table 3. The C1 content of SCB-HW was higher than SCB-GL and SCB-SC, and the C2 and C3 contents of SCB-HW were lower than SCB-GL and SCB-SC. The C1 content of SP-HW was higher than SP-GL and SP-SC, and the C2 and C3 contents of SP-HW were lower than SP-GL and SP-SC. These results indicated that the surface of hot water-pretreated CNF films had the high lignin content, the surface of sodium chlorite-pretreated CNF films had the low lignin content. The lignin content on the surface of the green liquor-pretreated CNF films was possibly correlated with small, soluble lignin fragments being reabsorbed on the surface of wood fibers during the green liquor pretreatment process [32]. The C2 and C3 contents of SCB-GL or SP-GL were higher than those of SCB-HW or SP-HW because more lignin was removed during the green liquor pretreatment process. The C2 and C3 contents of SCB-SC or SP-SC were higher than those of SCB-HW or SP-HW because lignin was removed by sodium chlorite, leading to more carbohydrates being exposed on the surface of CNFs. Furthermore, the increase in C3 content due to sodium chlorite increases oxygen-containing functional groups in fibers. These results were consistent with the XPS full spectrum analysis.

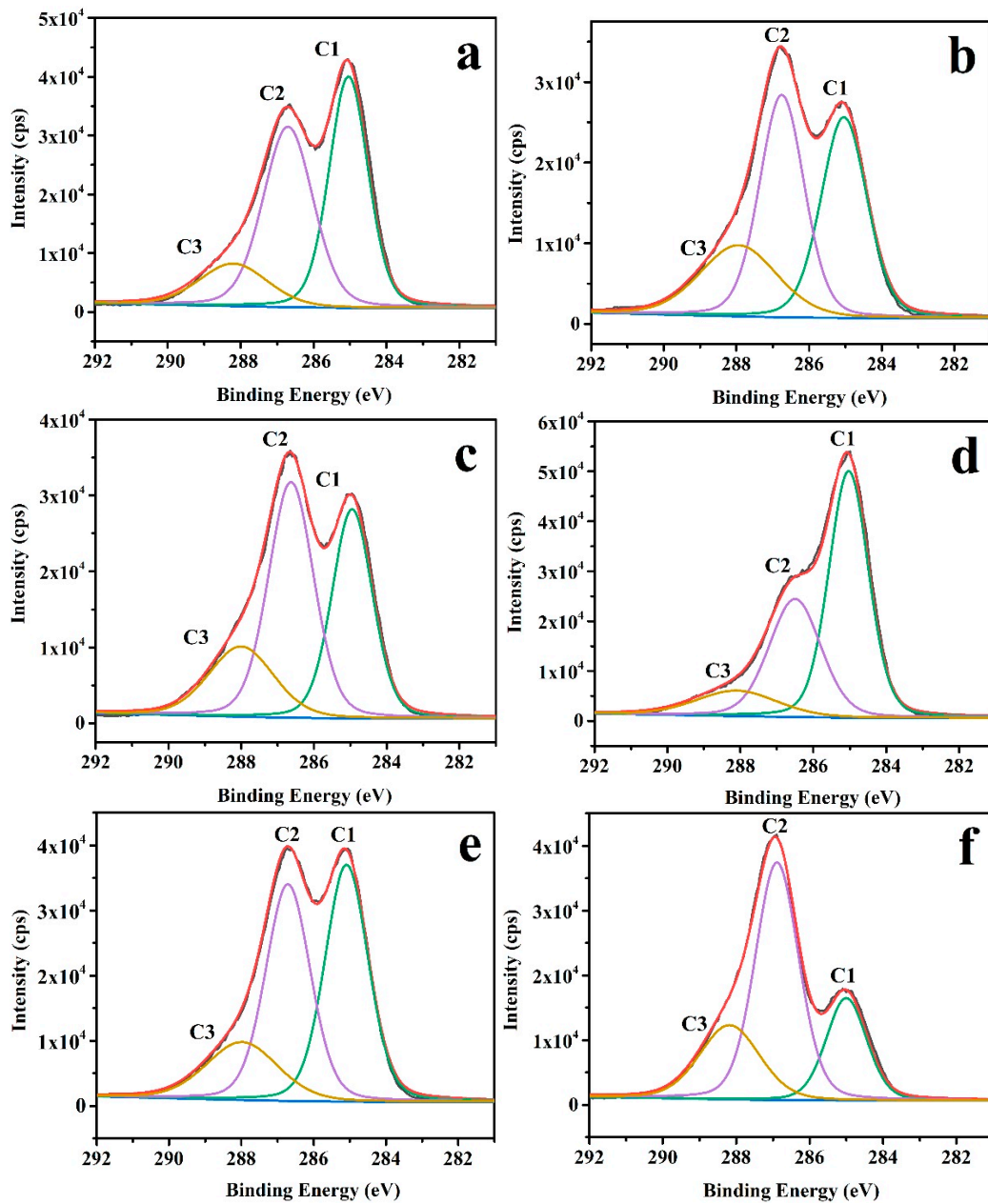


Figure 5. C1 s peaks of different CNFs films: (a) SCB-HW; (b) SCB-GL; (c) SCB-SC; (d) SP-HW; (e) SP-GL; (f) SP-SC.

Table 3. Elemental composition of C1s peak of CNFs films.

Samples	C1 (%)	C2 (%)	C3 (%)
SCB-HW	48.5	37.5	13.9
SCB-GL	39.5	42.4	18.2
SCB-SC	33.7	46.1	20.2
SP-HW	54.4	34.1	11.5
SP-GL	42.5	40.3	17.2
SP-SC	21.9	54.7	23.4

3.5. X-ray Diffraction (XRD) Analysis

The crystallinity of the pretreated sugarcane bagasse and spruce CNF films is shown in Figure 6. It can be seen that sugarcane bagasse and spruce before and after pretreatment have strong diffraction absorption peaks at $2\theta = 18^\circ$ and $2\theta = 22^\circ$, which indicate that the pretreated materials maintained the typical polymorphic form of cellulose I [47–49]. The

relative crystallinity of cellulose was calculated according to the Segal formula, as shown in Table 4.

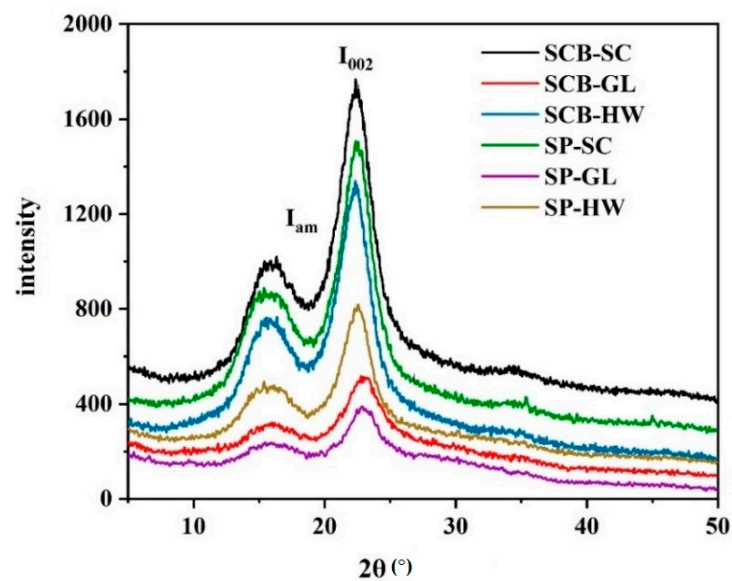


Figure 6. XRD analysis of CNFs films.

Table 4. Crystallinity of different CNFs films.

Samples	CrI (%)
SCB-HW	54.7 ± 0.5
SCB-GL	61.4 ± 0.7
SCB-SC	67.1 ± 0.4
SP-HW	51.2 ± 0.8
SP-GL	63.1 ± 0.4
SP-SC	65.5 ± 0.6

The crystallinities of SCB-HW and SP-HW were 54.72% and 51.23%, respectively, the crystallinities of SCB-GL and SP-GL were 61.35% and 63.09%, respectively, and the crystallinities of SCB-SC and SP-SC were 67.08% and 65.46%, respectively. It can be concluded that the crystallinity of the SC CNFs was higher than that of the hot water and green liquor pretreated CNFs because most of the lignin and hemicellulose were removed during the SC pretreatment process. The SCB-HW had higher crystallinity than SP-HW due to the removal of hemicellulose and lignin in sugarcane bagasse during the hot water pretreatment process was greater than that of spruce. Moreover, the aggregation state of cellulose and the supramolecular structure of cellulose formed a staggered combination of crystalline regions to amorphous regions. The cellulose molecular chains in the crystalline region have good orientation and high density and are not easily destroyed, while the cellulose chains in the amorphous region with poor orientation, disordered molecular arrangement, and irregular are easily destroyed [27]. After hot water pretreatment, the non-crystalline region of lignocellulose was destroyed, while the crystalline region of cellulose was relatively stable. Therefore, the proportion of the crystalline region of cellulose increased, finally leading to an increase in crystallinity. After green liquor pretreatment, the crystallinity of CNFs was higher than that of hot water-pretreated CNFs, possibly due to the lignin and hemicellulose in non-crystalline region were removed, and the molecular chain of the crystalline region of cellulose was broken to varying degrees under alkaline conditions.

3.6. Thermogravimetry (TGA) Analysis

The thermogravimetric analysis curves of different CNFs are shown in Figure 7, and the corresponding results are shown in Table 5. According to the change in mass loss shown in Figure 7a, the mass loss of CNFs at different temperatures can be divided into three regions. The temperature of region I ranged from 25 to 225 °C. The mass loss in this region was caused by the evaporation of water in the CNFs, and the average residual water was 5.64 wt.%. The temperature of region II ranged from 225 to 390 °C, which was the main stage of thermal degradation of different CNF samples, and the mass loss changed. The mass of region II suddenly decreased due to the depolymerization of cellulose [50]. The temperature of region III ranged from 390 to 700 °C. The cellulose in this zone was further pyrolyzed into coke and graphite. At this stage, the thermal degradation of each sample was relatively stable, and the mass loss was reduced. The residual mass of each sample at region III was consistently near 11%.

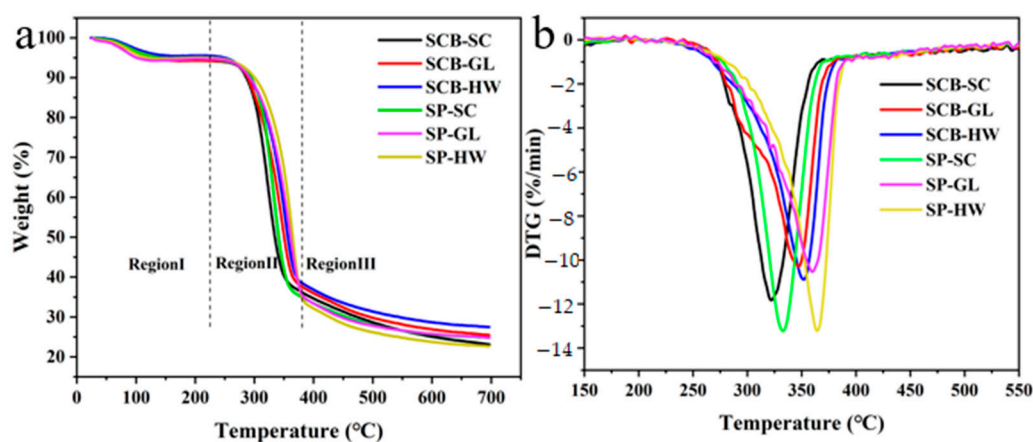


Figure 7. TG (a) and DTG (b) diagrams of different CNFs.

Table 5. Thermogravimetric analysis of different CNFs.

Sample	Region I		Region II		Region III	Tonset (°C)	Td (°C)
	Temperature (°C)	Residual Moisture (wt.%)	Temperature (°C)	Mass Residue (wt.%)	Mass Residue (wt.%)		
SCB-HW	251	5.11	387	38.11	10.63	297	352
SCB-GL	243	5.78	382	37.06	11.59	291	346
SCB-SC	255	6.51	369	37.23	14.11	284	323
SP-HW	252	5.50	392	32.86	10.20	321	364
SP-GL	240	5.45	385	33.97	9.13	320	360
SP-SC	239	5.49	372	35.68	10.87	301	333

The thermal stability of the SCB CNFs was as follows: SCB-HW > SCB-GL > SCB-SC. The thermal stability of the SP CNFs was as follows: SP-HW > SP-GL > SP-SC. Due to the high lignin content and the low hemicellulose content, there was a synergistic increase in the thermal stability of the CNFs. Furthermore, the thermal stability of SP-HW was higher than that of SCB-HW because the lignin content of SP-HW was higher than that of SCB-HW, and the hemicellulose contents of SP-HW and SCB-HW were basically equal. The thermogravimetric process of SP-GL as an example was analyzed in detail, as shown in Figure 7b. It can be concluded that when the heating temperature reached 240 °C, the free water of SP-GL CNFs was removed and began to undergo thermal degradation, resulting in a slight mass loss of SP-GL CNFs of 5.45%. When the temperature gradually increased to 320 °C, the mass loss of CNFs was obviously increased, and this temperature was defined as the initial degradation temperature (Tonset) of CNFs. When the temperature was continually raised to 360 °C, the mass of the CNFs rapidly degraded due to the formation

of volatile substances such as methane, carbon monoxide, and carbon dioxide [19]. This temperature was defined as the maximum thermal degradation temperature (Td) of CNFs. When the temperature reached 393 °C, the mass loss of CNFs remained stable, the thermal degradation also tended to be gentle, and the residual mass was 32.68%. According to the previous analysis, the two important indicators of thermal stability were Tonset and Td, and both indicators showed an upward trend because the degradation temperature of cellulose and hemicellulose was 350 °C. While the degradation temperature of lignin was above 400 °C, the thermal stability of lignin was better than that of cellulose and hemicellulose [51]. Because lignin had aromatic groups, ether and carbon–carbon bonds, these structures could not decompose at 350 °C. Although cellulose and hemicellulose can decompose at low temperatures, increasing the lignin content can improve the thermal stability of CNFs. Conclusively, the thermal stability of the different CNFs was directly correlated to the synergy of lignin and hemicellulose content of CNFs.

3.7. Analysis of UV Absorption Performance

The results of ultraviolet spectrum analysis of the CNF films are shown in Figure 8. The analysis showed that the transmittance of SCB-SC and SP-SC in 400–760 nm (visible light region) was higher than that of other pretreatments, which was consistent with the change in lignin content in CNFs [52] and the transparency effect of the CNF films. The UV resistance of the SCB-HW, SCB-GL, SP-HW, and SP-GL (190–400 nm) CNFs was near 100%, and the SCB-SC and SP-SC CNFs had low absorption rates of UV light due to the low lignin content in the SCB-SC and SP-SC CNFs. Furthermore, the functional groups of lignin can absorb UV light, such as phenol, ketone, and other chromophore groups, and the ultraviolet absorption of CNFs was correlated to the lignin content and functional group of lignin [34,53]. Conclusively, the high content of lignin in different pretreatment CNFs led to the high UV resistance of the CNFs.

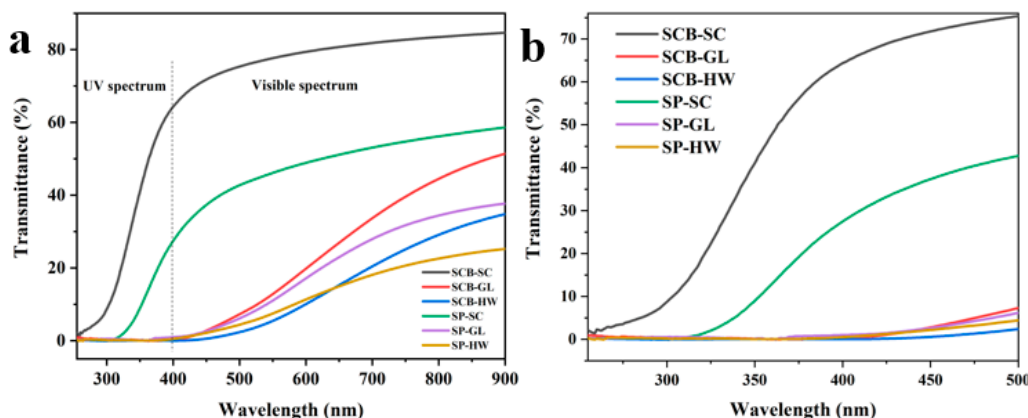


Figure 8. UV/Vis transmittance of different CNF films (a) 250–900 nm and (b) 200–500 nm.

4. Conclusions

Different pretreatment methods were used to pretreat sugarcane bagasse and spruce, and CNF films with different lignin and hemicellulose contents were prepared. Hot water pretreatment mainly removed the hemicellulose, and the green liquor mainly removed the lignin in the different CNFs. The thermal stability and UV resistance of all the spruce CNF films are higher than those of all the sugarcane bagasse CNF films. The thermal stability of the CNF films increased with increasing lignin content and decreasing hemicellulose content. The lignin content impacted the UV resistance of CNF films. Green liquor pretreatment can be used for the preparation of cellulose nanofibers. This study provides a theoretical basis for the application of lignin-containing cellulose nanofibers in thermal management and UV resistance fields.

Author Contributions: Conceptualization M.L.; methodology, M.L., X.W., and S.Z.; validation, L.L. and M.L.; formal analysis, X.W., S.Z., and X.Y.; investigation, X.W.; resources, L.L., M.L., and S.W.; data curation, X.W. and M.L.; writing—original draft preparation, X.W.; writing—review and editing, L.L., M.L., and S.W.; visualization, X.W.; supervision, L.L. and M.L.; project administration, L.L. and S.W.; funding acquisition, L.L. and S.W. All authors have read and agreed to the published version of the manuscript.

Funding: This work was supported by the National Natural Science Foundation of China (31660182) and the Natural Science Foundation Project of Guangxi (2018GXNSFAA281336).

Institutional Review Board Statement: Not applicable.

Informed Consent Statement: Not applicable.

Data Availability Statement: Data available in a publicly accessible repository.

Acknowledgments: Thanks for the Guangxi Key Laboratory of Clean Pulp & Papermaking and Pollution Control provided the technology and financial support.

Conflicts of Interest: The authors declare no conflict of interest.

References

1. Thomas, B.; Raj, M.C.; Athira, K.B.; Rubiyah, M.H.; Joy, J.; Moores, A.; Drisko, G.L.; Sanchez, C. Nanocellulose, a versatile green platform: From biosources to materials and their applications. *Chem. Rev.* **2018**, *118*, 11575–11625. [[CrossRef](#)] [[PubMed](#)]
2. Wang, L.; Fu, H.; Liu, H.; Yu, K.; Wang, Y.; Ma, J. In-situ packaging ultra-uniform 3D hematite nanotubes by polyaniline and their improved gas sensing properties. *Mater. Res. Bull.* **2018**, *107*, 46–53. [[CrossRef](#)]
3. Farooq, A.; Jiang, S.; Farooq, A.; Naeem, M.A.; Ahmad, A.; Liu, L. Structure and properties of high quality natural cellulose nano fibrils from a novel material Ficus natalensis barkcloth. *J. Ind. Text.* **2019**, 1–17. [[CrossRef](#)]
4. Mariano, M.; Cercená, R.; Soldi, V. Thermal characterization of cellulose nanocrystals isolated from sisal fibers using acid hydrolysis. *Ind. Crop. Prod.* **2016**, *94*, 454–462. [[CrossRef](#)]
5. Zhang, N.; Tao, P.; Lu, Y.; Nie, S. Effect of lignin on the thermal stability of cellulose nanofibrils produced from bagasse pulp. *Cellulose* **2019**, *26*, 7823–7835. [[CrossRef](#)]
6. Li, S.; Lee, P.S. Development and applications of transparent conductive nanocellulose paper. *Sci. Technol. Adv. Mater.* **2017**, *18*, 620–633. [[CrossRef](#)] [[PubMed](#)]
7. Liao, Q.; He, M.; Zhou, Y.; Nie, S.; Wang, Y.; Hu, S.; Yang, H.; Li, H.; Tong, Y. Highly cuboid-shaped heterobimetallic metal-organic frameworks derived from porous Co/ZnO/C microrods with improved electromagnetic wave absorption capabilities. *ACS Appl. Mater. Interfaces* **2018**, *10*, 29136–29144. [[CrossRef](#)]
8. Oikonomou, E.K.; Christov, N.; Cristobal, G.; Bourgaux, C.; Heux, L.; Boucenna, I.; Berret, J.F. Design of eco-friendly fabric softeners: Structure, rheology and interaction with cellulose nanocrystals. *J. Colloid Interface Sci.* **2018**, *525*, 206–215. [[CrossRef](#)]
9. Wu, X.; Li, S.; Coumes, F.; Darcos, V.; Him, J.L.K.; Bron, P. Modeling and self-assembly behavior of PEG-PLA-PEG triblock copolymers in aqueous solution. *Nanoscale* **2013**, *5*, 9010–9017. [[CrossRef](#)] [[PubMed](#)]
10. Tao, P.; Wu, Z.; Xing, C.; Zhang, Q.; Wei, Z.; Nie, S. Effect of enzymatic treatment on the thermal stability of cellulose nanofibrils. *Cellulose* **2019**, *26*, 7717–7725. [[CrossRef](#)]
11. Lin, X.; Wu, Z.; Zhang, C.; Liu, S.; Nie, S. Enzymatic pulping of lignocellulosic biomass. *Ind. Crop. Prod.* **2018**, *120*, 16–24. [[CrossRef](#)]
12. Huang, C.; Dong, H.; Su, Y.; Wu, Y.; Narron, R.; Yong, Q. Synthesis of carbon quantum dot nanoparticles derived from byproducts in bio-refinery process for cell imaging and in vivo bioimaging. *Nanomaterials* **2019**, *9*, 387. [[CrossRef](#)] [[PubMed](#)]
13. Atifi, S.; Miao, C.; Hamad, W.Y. Surface modification of lignin for applications in polypropylene blends. *J. Appl. Polym. Sci.* **2017**, *134*, 45103–45112. [[CrossRef](#)]
14. Cusola, O.; Rojas, O.J.; Roncero, M.B. Lignin particles for multifunctional membranes, antioxidative microfiltration, patterning, and 3D structuring. *ACS Appl. Mater. Interfaces* **2019**, *11*, 45226–45236. [[CrossRef](#)]
15. Rukmanikrishnan, B.; Rajasekharan, S.K.; Lee, J. K-carrageenan/lignin composite films: Biofilm inhibition, antioxidant activity, cytocompatibility, UV and water barrier properties. *Mater. Today Commun.* **2020**, *24*, 101346–101355. [[CrossRef](#)]
16. Nair, S.S.; Yan, N. Effect of high residual lignin on the thermal stability of nanofibrils and its enhanced mechanical performance in aqueous environments. *Cellulose* **2015**, *22*, 3137–3150. [[CrossRef](#)]
17. Vanholme, R.; Storme, V.; Vanholme, B. A systems biology view of responses to lignin biosynthesis perturbations in Arabidopsis. *Plant Cell* **2012**, *24*, 3506–3529. [[CrossRef](#)] [[PubMed](#)]
18. DeMartini, J.D.; Pattathil, S.; Miller, J.S. Investigating plant cell wall components that affect biomass recalcitrance in poplar and switchgrass. *Energy Environ. Sci.* **2013**, *6*, 898–909. [[CrossRef](#)]
19. Isaac, A.; de Paula, J.; Viana, C.M. From nano- to micrometer scale: The role of microwave-assisted acid and alkali pretreatments in the sugarcane biomass structure. *Biotechnol. Biofuels* **2018**, *11*, 73. [[CrossRef](#)]

20. Chirayil, C.J.; Mathew, L.; Thomas, S. Review of recent research in nano cellulose preparation from different lignocellulosic fibers. *Rev. Adv. Mater. Sci.* **2014**, *37*, 20–28.
21. Qing, Y.; Yi, J.; Wu, Y.; Cai, Z.; Wu, Q. Research progress in cellulose nanofiber films. *Trans. China Pulp. Pap.* **2016**, *31*, 55–62.
22. Lê, H.Q.; Dimic-Misic, K.; Johansson, L.; Maloney, T.; Sixta, H. Effect of lignin on the morphology and rheological properties of nanofibrillated cellulose produced from γ -valerolactone/water fractionation process. *Cellulose* **2018**, *25*, 179–194. [[CrossRef](#)]
23. Herrera, M.; Thitiwutthisakul, K.; Yang, X.; Rujitanaroj, P.; Rojas, R.; Berglund, L. Preparation and evaluation of high-lignin content cellulose nanofibrils from eucalyptus pulp. *Cellulose* **2018**, *25*, 3121–3133. [[CrossRef](#)]
24. Jiang, Y.; Liu, X.; Yang, Q.; Song, X.; Qin, C.; Wang, S.; Li, K. Effects of residual lignin on composition, structure and properties of mechanically defibrillated cellulose fibrils and films. *Cellulose* **2019**, *26*, 1577–1593. [[CrossRef](#)]
25. Wongjaiyen, T.; Brostow, W.; Chonkaew, W. Tensile properties and wear resistance of epoxy nanocomposites reinforced with cellulose nanofibers. *Polym. Bull.* **2017**, *75*, 2039–2051. [[CrossRef](#)]
26. Zainuddin, S.Y.; Ahmad, I.; Kargarzadeh, H. Potential of using multiscale kenaf fibers as reinforcing filler in cassava starch-kenaf biocomposites. *Carbohydr. Polym.* **2013**, *92*, 2299–2305. [[CrossRef](#)] [[PubMed](#)]
27. Li, M.; Guo, C.; Luo, B. Comparing impacts of physicochemical properties and hydrolytic inhibitors on enzymatic hydrolysis of sugarcane bagasse. *Bioprocess Biosyst. Eng.* **2020**, *43*, 111–122. [[CrossRef](#)]
28. Jiang, B.; Wang, W.; Gu, F.; Cao, T.; Jin, Y. Comparison of the substrate enzymatic digestibility and lignin structure of wheat straw stems and leaves pretreated by green liquor. *Bioresour. Technol.* **2016**, *199*, 181–187. [[CrossRef](#)] [[PubMed](#)]
29. BH Sluiter, A.; Hames, B.; Ruiz-Peinado, R.; Scarlata, C.; Sluiter, W.J.; Templaton, D.; Crocker, A.; Sluiter, M.D. Determination of structural carbohydrates and lignin in biomass. *Natl. Renew. Energy Lab.* **2008**, *510*, 1–16.
30. Herrera-Morales, J.; Turley, T.A.; Betancourt-Ponce, M.; Nicolau, E. Nanocellulose-block copolymer films for the removal of emerging organic contaminants from aqueous solutions. *Materials* **2019**, *12*, 230. [[CrossRef](#)]
31. Chen, Y.W.; Hasanulbasori, M.A.; Chiat, P.F.; Lee, H.V. Pyrus pyrifolia fruit peel as sustainable source for spherical and porous network based nanocellulose synthesis via one-pot hydrolysis system. *Int. J. Biol. Macromol.* **2019**, *123*, 1305–1319. [[CrossRef](#)]
32. Yue, Z.; Hou, Q.; Liu, W.; Yu, S. Autohydrolysis prior to poplar chemi-mechanical pulping: Impact of surface lignin on subsequent alkali impregnation. *Bioresour. Technol.* **2019**, *282*, 318–324. [[CrossRef](#)]
33. Segal, L.; Creely, J.J.; Martin, A.E.; Conrad, C.M. An empirical method for estimating the degree of crystallinity of native cellulose using the X-ray diffractometer. *Text. Res. J.* **1959**, *29*, 786–794. [[CrossRef](#)]
34. Bian, H.; Gao, Y.; Wang, R.; Liu, Z.; Wu, W.; Dai, H. Contribution of lignin to the surface structure and physical performance of cellulose nanofibrils film. *Cellulose* **2018**, *25*, 1309–1318. [[CrossRef](#)]
35. Errokh, A.; Magnin, A.; Putaux, J.L.; Boufi, S. Hybrid nanocellulose decorated with silver nanoparticles as reinforcing filler with antibacterial properties. *Mater. Sci. Eng. C Mater. Biol. Appl.* **2019**, *105*, 110044. [[CrossRef](#)]
36. Hong, S.; Song, Y.; Yuan, Y. Production and characterization of lignin containing nanocellulose from luffa through an acidic deep eutectic solvent treatment and systematic fractionation. *Ind. Crop. Prod.* **2020**, *143*, 111913. [[CrossRef](#)]
37. Sim, S.F.; Mohamed, M.; Lu, N.; Sarman, N.S.P.; Samsudin, S.N.S. Computer-assisted analysis of fourier transform infrared (ftir) spectra for characterization of various treated and untreated agriculture biomass. *Bioresources* **2012**, *7*, 5367–5380. [[CrossRef](#)]
38. Sun, B.; Zhang, Y.; Li, W.; Xu, X.; Zhang, H.; Zhao, Y.; Lin, J.; Sun, D. Facile synthesis and light-induced antibacterial activity of ketoprofen functionalized bacterial cellulose membranes. *Colloids Surf. A Physicochem. Eng. Asp.* **2019**, *568*, 231–238. [[CrossRef](#)]
39. Zhang, X.; Sun, H.; Tan, S.; Gao, J.; Fu, Y.; Liu, Z. Hydrothermal synthesis of Ag nanoparticles on the nanocellulose and their antibacterial study. *Inorg. Chem. Commun.* **2019**, *100*, 44–50. [[CrossRef](#)]
40. Hsu, T.C.; Guo, G.L.; Chen, W.H.; Hwang, W.S. Effect of dilute acid pretreatment of rice straw on structural properties and enzymatic hydrolysis. *Bioresour. Technol.* **2010**, *101*, 4907–4913. [[CrossRef](#)] [[PubMed](#)]
41. Zhang, S.; Zhang, F.; Jin, L.; Liu, B.; Mao, Y.; Liu, Y.; Huang, J. Preparation of spherical nanocellulose from waste paper by aqueous NaOH/thiourea. *Cellulose* **2019**, *26*, 5177–5185. [[CrossRef](#)]
42. Hamed, S.A.A.K.M.; Hassan, M.L. A new mixture of hydroxypropyl cellulose and nanocellulose for wood consolidation. *J. Cult. Herit.* **2019**, *35*, 140–144. [[CrossRef](#)]
43. Gan, I.; Chow, W.S. Synthesis of phosphoric acid-treated sugarcane bagasse cellulose nanocrystal and its thermal properties enhancement for poly(lactic acid) nanocomposites. *J. Thermoplast. Compos. Mater.* **2018**, *32*, 619–634. [[CrossRef](#)]
44. Li, M.; Yin, J.; Hu, L.; Chen, S.; Min, D.; Wang, S.; Luo, L. Effect of hydrogen peroxide bleaching on anionic groups and structures of sulfonated chemo-mechanical pulp fibers. *Colloids Surf. A Physicochem. Eng. Asp.* **2020**, *585*, 124060–124068. [[CrossRef](#)]
45. Koljonen, K.; Österberg, M.; Johansson, L.S.; Stenius, P. Surface chemistry and morphology of different mechanical pulps determined by ESCA and AFM. *Colloids Surf. A Physicochem. Eng. Asp.* **2003**, *228*, 143–158. [[CrossRef](#)]
46. Hon, D.N.-S. ESCA study of oxidized wood surfaces. *J. Appl. Polym. Sci.* **1984**, *2777*–2784. [[CrossRef](#)]
47. Supian, M.A.F.; Amin, K.N.M.; Jamari, S.S.; Mohamad, S. Production of cellulose nanofiber (CNF) from empty fruit bunch (EFB) via mechanical method. *J. Environ. Chem. Eng.* **2020**, *8*, 103020–103024. [[CrossRef](#)]
48. French, A.D. Idealized powder diffraction patterns for cellulose polymorphs. *Cellulose* **2014**, *21*, 885–896. [[CrossRef](#)]
49. Gwon, J.G.; Lee, S.Y.; Doh, G.H.; Kim, J.H. Characterization of chemically modified wood fibers using FTIR spectroscopy for biocomposites. *J. Appl. Polym. Sci.* **2010**, *116*, 3212–3219. [[CrossRef](#)]
50. Trilokesh, C.; Uppuluri, K.B. Isolation and characterization of cellulose nanocrystals from jackfruit peel. *Sci. Rep.* **2019**, *9*, 16702–16709. [[CrossRef](#)] [[PubMed](#)]

51. Peng, Y.; Nair, S.S.; Chen, H.; Yan, N.; Cao, J. Effects of lignin content on mechanical and thermal properties of polypropylene composites reinforced with micro particles of spray dried cellulose nanofibrils. *ACS Sustain. Chem. Eng.* **2018**, *6*, 11078–11086. [[CrossRef](#)]
52. Hambarzumyan, A.; Foulon, L.; Chabbert, B.; Aguié-Beghin, V. Natural organic UV-absorbent coatings based on cellulose and lignin: Designed effects on spectroscopic properties. *Biomacromolecules* **2012**, *13*, 4081–4088. [[CrossRef](#)] [[PubMed](#)]
53. Habibi, Y.; Lucia, L.A.; Rojas, O.J. Cellulose nanocrystals: Chemistry, self-assembly, and applications. *Chem. Rev.* **2010**, *110*, 3479–3500. [[CrossRef](#)] [[PubMed](#)]